Computer Controlled Bipolar Pulse Conductivity System for Applications in Chemical Rate Determinations

ARTICLE *in* ANALYTICAL CHEMISTRY · SEPTEMBER 1978

Impact Factor: 5.64 · DOI: 10.1021/ac50033a037

4 AUTHORS, INCLUDING:

Jim Holler
University of Kentucky
19 PUBLICATIONS **213** CITATIONS
SEE PROFILE

Stanley R. Crouch
Michigan State University
155 PUBLICATIONS **2,547** CITATIONS
SEE PROFILE

Chris Enke
University of New Mexico
198 PUBLICATIONS **4,630** CITATIONS
SEE PROFILE

(2) R. K. Kobos, and G. A. Rechnitz, *Anal. Lett.*, **10**, 751 (1977).
(3) G. A. Rechnitz, R. K. Kobos, S. J. Riechel, and C. R. Gebauer, *Anal. Chim. Acta*, **94**, 357 (1977).
(4) P. D'Orazio and G. A. Rechnitz, *Anal. Chem.*, **49**, 2083 (1977).
(5) T. Imoto, L. N. Johnson, A. C. T. North, P. C. Phillips, and J. A. Rupley in "The Enzymes", Vol. VII, P. D. Boyer, Ed., Academic Press, New York, N.Y., 1972, Chapter 21.
(6) M. Frobisher, R. D. Hinsdill, K. T. Crabtree, and C. K. Goodheart, "Fundamentals of Microbiology", 9th ed., W. B. Saunders Co., Philadelphia, Pa., 1974, Chapter 14.
(7) J. A. Demetriou, P. A. Drewes, and J. B. Gin in "Clinical Chemistry, Principles and Technics", 2nd ed., R. J. Henry, D. C. Cannon, and J. W. Winkleman, Ed., Harper and Row, Hagerstown, Md., 1974, Chapter 21.
(8) M. Meyerhoff and G. A. Rechnitz, *Science*, **195**, 494 (1977).
(9) G. J. Moody and J. D. R. Thomas, "Selective Ion Sensitive Electrodes", Merrow, Watford, England, 1971, Chapter 2.
(10) Sigma Catalog, Sigma Chemical Co., St. Louis, Mo., April 1977.
(11) Catalogue of Strains I, The American Type Culture Collection, Rockville, Md., 1976.
(12) S. D. Cosloy and M. Oishi, *Mol. Gen. Genet.*, **124**, 1 (1973).
(13) M. Mandel and A. Higa, *J. Mol. Biol.*, **53**, 159 (1970).
(14) M. Ariel and N. Grossowicz, *Biochim. Biophys. Acta*, **352**, 122 (1974).
(15) K. Cammann, *Fresenius Z. Anal. Chem.*, **257** 1 (1977).
(16) R. C. Davies, A. Neuberger, and B. M. Wilson, *Biochim. Biophys. Acta*, **178**, 294 (1969).

RECEIVED for review April 10, 1978. Accepted June 28, 1978. We gratefully acknowledge the support of a grant from the National Institutes of Health.

Computer Controlled Bipolar Pulse Conductivity System for Applications in Chemical Rate Determinations

K. J. Caserta

Ivorydale Technical Center, The Procter and Gamble Company, Cincinnati, Ohio 45217

F. J. Holler*

Department of Chemistry, University of Kentucky, Lexington, Kentucky 40506

S. R. Crouch and C. G. Enke

Department of Chemistry, Michigan State University, East Lansing, Michigan 48824

A computer-controlled bipolar pulse conductivity system has been developed for use as a detector in chemical rate determinations. The instrument has a wide dynamic range (10^{-1}–10^{-8} Ω^{-1}), and it exhibits signal-to-noise ratios of up to 6×10^3 for a single data acquisition and 6×10^5 for ensemble averages of 2000 acquisitions. The accuracy of the system depends on several instrumental factors and ranges from 1% to 0.005% without calibration. With calibration against suitable standards, the worst-case error is 0.02%. The system is capable of performing discrete conductance measurements in 30 μs when operating at its maximum data rate. The speed and utility of the instrument are demonstrated by its use as the detection system in stopped-flow studies of the dehydration of carbonic acid and the reaction of nitromethane with base. Numerical correction of the data for temperature changes which occur in the conductance cell is also illustrated.

Traditionally, the measurement of electrolytic conductance has been one of the most accurate and precise of all electrochemical techniques. Unfortunately, the laborious procedures often required to achieve such measurements have hindered its routine use in the analytical laboratory and its use in conjunction with other techniques such as stopped-flow mixing which require rapid response. The electronic revolution of the past decade has made possible new instrumental methods which previously were difficult or impossible to carry out. Among these is the bipolar pulse technique which was first developed in our laboratories (*1*). The technique involves the sequential application of two voltage pulses of equal magnitude and duration but opposite polarity to a cell, followed by measurement of the instantaneous cell current at the exact end of the second pulse. In this way the voltage across the series capacitance of the cell electrodes is nearly zero and the parallel capacitances associated with the conductivity cell and connections are drawing essentially no current at the time of measurement. A determination of the cell current at this time, therefore, allows an accurate measurement of the cell resistance. The measurement itself is then subject only to the limitations of the particular instrument and not to the cell design, chemical application, or solvent system employed. Subsequent work with this technique has demonstrated its wide dynamic range and sensitivity for various conductometric measurement problems (*2*, *3*), and variations on the technique have been developed by others (*4*, *5*).

In the sections which follow, we present a completely automatic computerized version of the bipolar pulse instrument which features: computer control over the analog portions of the circuit; high speed readjustment of circuit parameters (<300 μs); optimization of each measurement in real-time; signal-to-noise enhancement by averaging and digital smoothing; rapid and sophisticated data analysis; and correction for temperature changes which may occur during the measurement process. The instrument is entirely under the control of the computer system, and it requires no manual manipulation of circuit parameters. The tremendous flexibility of the instrumental system is demonstrated by employing it as the detection system in a stopped-flow mixing apparatus. As examples of the types of chemical systems that can be studied with such an apparatus, fundamental investigations of the dehydration of carbonic acid and of the pseudo-first-order reaction of nitromethane with base are presented.

THE INSTRUMENT

A block diagram of the instrument system is shown in Figure 1. It includes the computer, the computer peripherals, and the bipolar pulse instrument. The computer is a Digital Equipment Corporation (DEC) PDP 8/e with 16K of memory. The peripherals available include a dual floppy disk system, a cartridge disk system, an extended arithmetic element, a mainframe real

0003-2700/78/0350-1534$01.00/0

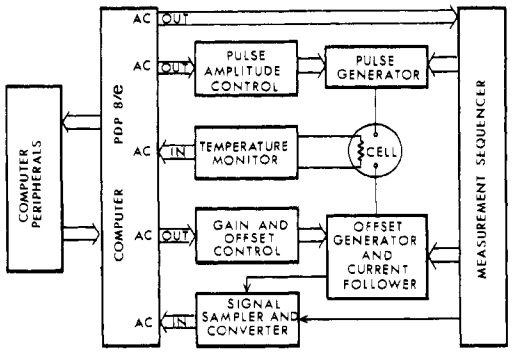

Figure 1. Block diagram of the computerized conductance instrument

time clock, a DECwriter, and a graphics display terminal. The Heath EU-801E interface system was used. The structure of the conductance instrument was organized to take advantage of the interactions available with this computer sysem. The DEC OS/8 operating system was used for software development and program execution. All programming was carried out using the FORTRAN II compiler and the SABR assembler provided by DEC. The hardware was specifically designed to utilize the software available in OS/8.

The instrument is controlled by data transferred from the computer to the control circuits and the measurement sequencer. The computer can also supply the triggering signal to the measurement sequencer which initiates pulsing. The pulse amplitude control module receives data from the CPU which determines the pulse height and provides the correct positive and negative voltage levels to the pulse generator. The gain and offset controls determine the amplification of the signal produced by pulsing the cell and the amount of that signal offset before amplification. The measurement sequencer, which supplies the signals that determine the length of the pulses and the timing of the measurement, contains a computer controlled time base. The analog signal produced by the combination of the cell and offset currents is tracked, held, and converted to a digital signal by the signal sampler and converter under control of the measurement sequencer. Finally, the digital information is transferred to the computer under software control and stored for later analysis.

Cell temperature may be simultaneously followed by the computerized temperature monitor which has been described elsewhere (*6*).

The Analog Interactions. Since the present instrument was specifically designed for computer control and monitoring, it was possible to simplify the analog circuits by use of digital circuit adjustment techniques and a digital data acquisition system.

The simplified schematic diagram of Figure 2 illustrates the interaction of the computer with the analog portion of the circuit. All of the precision voltages necessary for the operation of the instrument are derived from the precision +5 V and −5 V supplies which are regulated to 0.01%. These voltages are the inputs to the two voltage divider circuits of the pulse amplitude control shown inside the dashed line of the figure. The computer selects the amplitude of the bipolar pulse (±5, ±0.5, or ±0.05 V) by switching on one of the three DPST relays (C, D, or E). The pulse generator, amplifier A3, applies the chosen positive and negative pulses to the cell. Pulsing occurs during the timing sequence A–B–C on the switch control waveforms POS, NEG, and BOTH shown in Figure 2. The polarity of the pulse is determined by the state of field effect transistor (FET) switch X under control of the measurement sequencer waveform POS. The polarity is positive during time A–B and negative at all other times. The output of amplifier A3 is connected to the cell during the total pulsing time (A–C) by FET switch Y which is controlled by measurement sequencer waveform BOTH. Four cell leads are used: two to maintain the cell at the chosen voltage level and two to supply current for the cell. This arrangement reduces the effect of contact resistance to the cell leads. Amplifier A4 is a very fast (500 V/μs) current follower which also controls the lower electrode to be at virtual ground and sinks all currents to virtual ground when pulses are not being applied by connection to FET switch Y. When the current output of the cell is not being monitored, a 500-Ω resistor is switched into the feedback loop of amplifier A4 by FET switch Z to ensure that the inverting input will be at virtual ground, and to prevent amplifier saturation during the positive pulse. During the time interval B–C (NEG), when the cell current is being sampled, the appropriate computer-selected feedback resistance is switched into the circuit by FET switch Z under control of the measurement sequencer. The current follower output is divided to give a signal, E_s, to the sample and hold module, which is $^4/_5$ of the actual output. To the analog circuit, then, the 0–10 volt analog-to-digital converter (ADC) appears to be a 0–12.5 volt converter. This was done to provide overlap at scale changes which eliminates the need for precise scale adjustments, as will be explained in the Performance section. The voltage output, E_s, is tracked and held at the exact end of the second pulse by the signal sampler and converter.

In order to provide additional resolution most of the cell current can be offset by a constant current supplied by operational

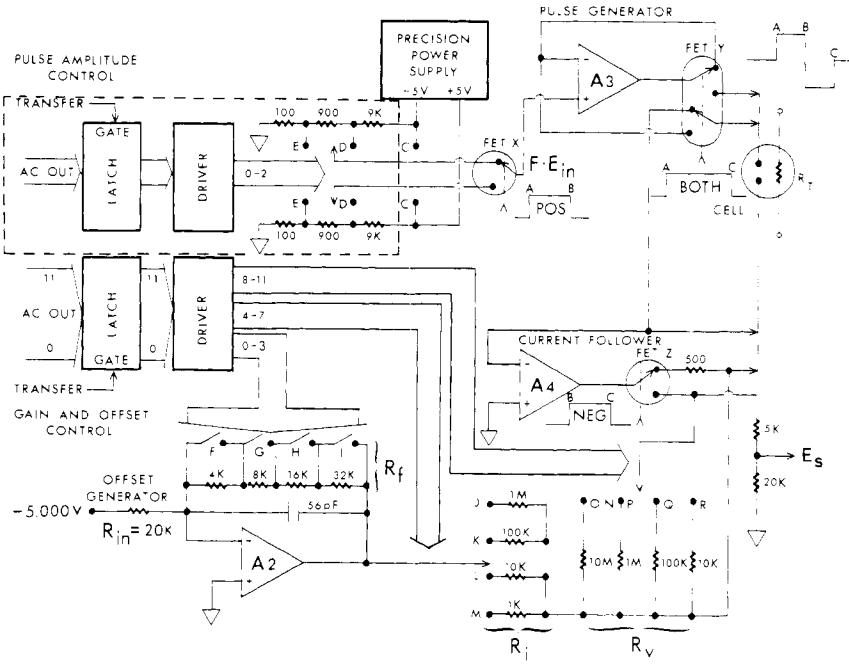

Figure 2. Analog circuits of the conductance instrument

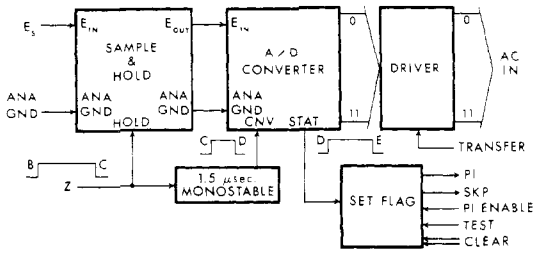

Figure 3. Analog-to-digital conversion section of the conductance instrument

amplifier A2. The required amount of offset is selected by the computer through appropriate combination of feedback resistors and series resistors (relays F–M). The offset current produced is added to the cell current at the summing point of amplifier A4 producing up to four additional most-significant bits of resolution in the conversion process (*7*).

The Digital Interactions. The digital measurement of the conductance information at the output of the current follower is made by the combination of a fast tracking sample-and-hold module and a 10-μs, 12-bit ADC. Waveform NEG from the measurement sequencer causes the sample and hold module shown in Figure 3 to track during the negative pulse and hold the signal, E_s, at the exact end of the pulse (time C). The falling edge of waveform NEG triggers a 1.5-μs monostable which resets the ADC on its rising edge and initiates conversion on the falling edge at time D. The status output of the converter sets a skip flag at the end of conversion (time E) and, if desired, a program interrupt. The output of the ADC is transferred to the computer upon request. The flag is read and cleared by the computer and is automatically cleared at the start of the program.

It has been pointed out (*1*, *2*) that the timing of pulses is critical to the success of a conductance measurement using the bipolar pulse technique. Thus, the precise internal timing system shown in Figure 4 was utilized to produce the waveforms. A synchronous 2-bit counter driven by a crystal oscillator–multiplexer is used to generate the POS, NEG, and BOTH waveforms shown in Figures 2, 3, and 4. The frequency of the single-cycle pulse generator is under computer control, and it may be triggered by the computer or an external event generated by another instrument. Decade values of pulse widths from 10 μs to 100 s are available, but only those from 10 μs to 10 ms are useful for real conductance cells.

System Flexibility and Software. The component circuits of the instrument provide the sequence of events necessary to perform a measurement of conductance. These circuits are directly interconnected (hardware connection) only to the extent required by these sequences. Most interactions are performed through the computer software, thus producing a high degree of flexibility within the instrumental system. The placement of the computer's decision-making abilities within the instrumental framework allows interactions between the various separate circuits that are intelligent or responsive rather than fixed. In this way, the instrument may be altered to perform a new mode of chemical measurement by a simple modification of the control software. The experiment itself may then be reconfigured during run time through the software–instrument–experiment correlation in such a way that the data collected are the optimum data attainable by the technique.

The software for the computerized conductance instrument may be broadly classified into three categories: utility routines, data acquisition routines, and data analysis routines. A common element in both the utility and data acquisition categories is the preliminary routine which determines the optimum circuit settings for each of the four useful pulse widths according to the optimization rules which are discussed in another section. Utility routines are available for the determination of signal-to-noise ratios, of accuracy with respect to standards, of optimum pulse width, and of optimum pulse timing. In addition, routines are available for periodic exercising and maintenance of the circuits.

The data acquisition routines include facility for the acquisition of a single signal average of a given number of discrete data points or of a specific number of such signal averages at precisely timed intervals. Additionally, it is possible to acquire and analyze data continuously at precisely timed intervals and output the data to the console device or to the DECwriter. A maximum data rate mode is also available for chemical processes which occur on a very fast time scale. A multiple data rate routine may be used to provide useful conductance information on both long and short time scales. Finally, in each data acquisition routine, it is possible to acquire temperature and conductance data concurrently for use in correcting for temperature changes.

The data analysis routines vary somewhat with the type of experiment which is to be carried out, but most allow the following operations to be performed. Upon entry into the data analysis routine, the raw conductance data are calculated and stored in memory in preparation for subsequent manipulations. The operator may then choose to plot the data on the graphics display terminal, list it on the DECwriter, or correct it for temperature, dilution, or scale change effects. The data can also be stored in a file on the mass storage device for subsequent retrieval and analysis by the same or other programs.

The heart of each of the data analysis routines is an interactive graphics subroutine that enables the operator to specify particular points or regions on the G-vs.-time (or G-vs.-volume) curves for each experiment. The operator may then request the average conductance (G) or temperature (T) over a region of the curve, the values of G and T at the specified points, or other more complex results such as the end point in a titration, the first-order rate constant in a kinetics experiment, or a derivative smooth of either conductance or temperature data (*8*, *9*).

Measurement Optimization. An expression for the conductance, G, of the cell in the circuit of Figure 2 may be derived as follows:

$$G_{cell} = I_{cell}/E_{cell} \quad (1)$$

where

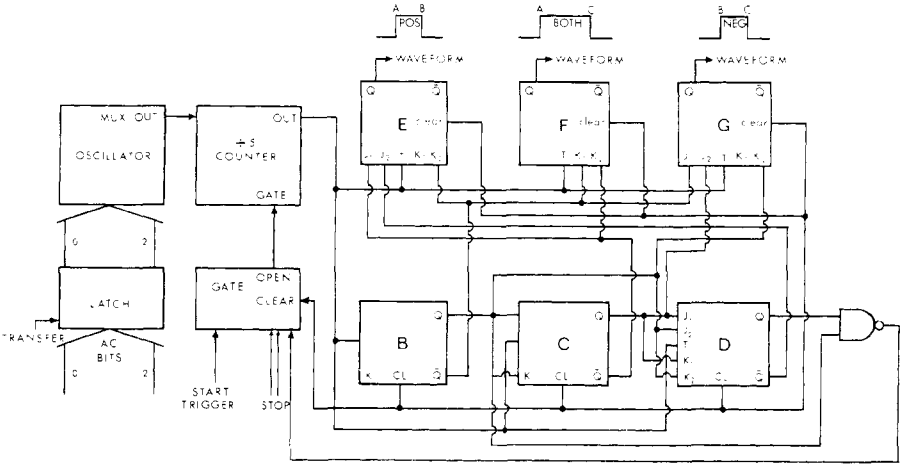

Figure 4. Measurement sequencer of the conductance instrument

$$I_{cell} = I_{measd} - I_{offset} \quad (2)$$

But

$$I_{measd} = (5/4)(E_s/R_v) \quad (3)$$

and

$$I_{offset} = R_f E_{in}/R_{in}R_i \quad (4)$$

where E_{in} = 5.000 V, and the factor (5/4) results from the voltage divider at the output of the circuit. Since $E_{cell} = E_{in}F$ where F is the pulse height multiplier determined by the voltage divider in the pulse amplitude control module, we then have

$$G_{cell} = (FE_{in})^{-1}[(5/4)(E_s/R_v) - (R_f E_{in}/R_{in}R_i)]$$
$$= F^{-1}[(5/4)(E_s/E_{in}R_v) - (R_f/R_{in}R_i)] \quad (5)$$

Obviously, for a given conductance, a number of circuit settings could be chosen which would yield a signal within the range of the ADC. Since estimates of the uncertainties of each component in the above equation are known, it is possible to calculate the error in the measured conductance for each different instrument setting and various values of E_s. A computer program was written to perform this task, and the results indicated that maximum accuracy could be attained at maximum pulse height, minimum feedback resistance in the current follower, maximum offset, and maximum E_s.

Based on these rules, an algorithm was built into the preliminary routine which maximizes resolution and accuracy by increasing the pulse height to its maximum value and then, if necessary, increasing the current follower gain until the ADC overranges. Current offset is then applied until the ADC is back on scale, thus providing the MSBs of the analog-to-digital conversion. This process is carried out at each of the four pulse widths, and the circuit parameters for each are stored for later use. If the circuit parameters cannot be optimized, the appropriate error messages are output to the console device. These optimization rules are also used in the data acquisition routines at run time to maintain the instrument response within the range of the ADC. If, in the data acquisition routine, the ADC is found to be off-scale, an optimization routine is entered which changes the circuit parameters in the fastest possible manner to bring the response on-scale, and the change in the parameters is recorded in memory for the eventual calculation of G. Through the use of these algorithms, the bipolar pulse conductance system always makes the best measurement that is consistent with the quality of the components of the system.

PERFORMANCE

Scale Changes. The instrument, as initially designed, performed well over its entire range except in the regions of scale changes. It was found to be impossible to align perfectly the pulse height, current follower gain, and offset so that there were no discontinuities on changing the various scaling parameters. The use of the four-fifths voltage divider at the output of A4 provides ample overlap between ranges so that the computer does not "hunt" or lose data. In addition, the problem of some nonlinearity at the lowest current follower (A4) output was solved by not allowing an A/D conversion below 0077_8 without a scale change. Any discontinuity occurring at the scale change was eliminated by allowing the computer to adjust mathematically the data at those points. The data acquisition routine stores parameters corresponding to the settings of the analog circuit for each measured conductance. When the data analysis routine senses a scale change, it computes and stores the difference between the value of the conductance before the scale change and the value after the scale change. This difference is then added to all subsequent measurements of conductance. It was found that the overlap combined with computer correction of data made instrumental adjustment virtually unnecessary. Only infrequent trimming of the current follower (A4), to prevent nonlinear response due to pulse asymmetry, is required.

Linearity and Range. Many of the operational amplifiers in the analog circuit have very fast response times and, thus, a tendency to oscillate. A 56-pF capacitor prevents oscillaltion of the offset amplifier (A2), but a small capacitor in the feedback loop of the current follower (A4) causes its response to become nonlinear. Occasionally, small 10-MHz oscillations are present at the output of A4. These oscillations have no effect on the measurement since the bandwidth of the instrument is upper-limited by the 500 KHz bandwidth of the sample-and-hold module.

For any scale setting within the operating range of the instrument, the true value of the resistance is equal to the sum of the measured resistance and a constant. The constant does not change over the range of any given scale. Thus, a simple correction algorithm provides linearity over the entire operating range of the instrument. The constant for any given scale setting may be calculated by measuring a single standard resistance which lies within that range as detailed below in the discussion of accuracy. The instrument is therefore linear over its entire operating range, which extends from 2.2×10^{-1} to 1.3×10^{-8} Ω^{-1}. Above 0.22 Ω^{-1}, the conductivity is so high that maximum offset is insufficient to put the conversion system on scale. Below 1.3×10^{-8} Ω^{-1}, conduction between the copper foil pattern through the glass epoxy printed circuit board becomes significant compared to the measured conductance.

Resolution and Signal-to-Noise Ratio. For measurements which do not involve averaging discrete data, the resolution is limited by the conversion system, the maximum being at 8 or more offset "units" applied, yielding 16 bits of resolution. At very low conductance where no offset is applied, 12 or less bits of conversion are obtained. To determine the signal-to-noise ratio (S/N), the instrument was connected to a set of standard resistors with 1 ppm/K temperature stability. One of the data acquisition routines was then used to acquire a set of ensemble averages, each consisting of a discrete number of points. The results of these experiments are listed in Table I.

As can be seen in Table I, averaging of data increases the S/N to quite large values and also provides additional bits of resolution as has been pointed out (*10*). The region of maximum S/N occurs around 10^{-3} Ω^{-1} where the noise on the signal (for an average of 2000 conductance data points per average) is only about 1.6 parts per million. All data represent sets of from 100 to 500 averages taken at close intervals. Some measurements were limited by the stability of the standards available.

Accuracy. In making absolute conductance measurements, a standard resistance is measured which requires the same instrumental scale settings as the conductance to be determined. Once the computer is given the true value of the standard, it can software correct any conductance measured at that scale setting since the error is constant for any chosen conductance and linear within a particular scale setting. Instrumental drift was found to be an insignificant problem (less than 0.005% per day) over most of the range of operation. In the lower conductance region (less than 2×10^{-7} Ω^{-1}) accuracy is limited by random errors caused by the relatively higher noise levels on the low current signals produced. In the highest conductance regions (greater than 10^{-1} Ω^{-1}), accuracy is limited by the relatively higher asymmetry in the lowest pulse height.

The accuracy was, however, found to be predominantly a function of the series capacitance associated with the cell as can be seen from Table II. This effect arises from pulse height asymmetry due to finite FET switching and amplifier settling times as well as the stability of the virtual ground maintained by the current follower. This stability decreases as the amount of current supplied to the summing point increases. The current reaches a maximum at the highest offset currents, corresponding to conductances of 2×10^{-3} Ω^{-1}, 2×10^{-4} Ω^{-1},

Table I. Performance Characteristics

conductance, Ω^{-1}	number of points/average	standard deviation	S/N ratio	limited by
4.9×10^{-2}	1	4.16×10^{-5}	1.18×10^{3}	noise
4.9×10^{-2}	2000	2.17×10^{-6}	2.26×10^{4}	limit of averaging
9.4×10^{-3}	1	1.41×10^{-5}	6.70×10^{3}	noise
9.4×10^{-3}	2000	3.23×10^{-8}	2.92×10^{5}	limit of averaging
9.9×10^{-4}	1	1.50×10^{-7}	6.60×10^{3}	noise
9.9×10^{-4}	2000	1.54×10^{-9}	6.40×10^{5}	stability of standard
3.2×10^{-4}	1	7.45×10^{-8}	4.34×10^{3}	noise
3.2×10^{-4}	2000	1.52×10^{-9}	2.13×10^{5}	stability of standard
9.9×10^{-5}	1	6.29×10^{-8}	1.43×10^{3}	noise
9.9×10^{-5}	2000	2.30×10^{-10}	4.20×10^{5}	limit of averaging
9.9×10^{-6}	1	6.74×10^{-9}	1.47×10^{3}	noise
9.9×10^{-6}	2000	3.60×10^{-11}	2.74×10^{5}	limit of averaging
8.2×10^{-7}	1	1.27×10^{-9}	6.40×10^{2}	noise
8.2×10^{-7}	2000	1.05×10^{-11}	7.77×10^{4}	stability of standard
9.0×10^{-8}	1000	9.96×10^{-12}	9.01×10^{3}	stability of standard, time scale of experiment

Table II. Inaccuracy (in percent) for Various Conductance-Series Capacitance Combinations[a]

	C, μF		
G, Ω^{-1}	10	5	1
10^{-1}	0.17	4.4	19
2×10^{-2}	0.0053	0.82	0.057
10^{-2}	0.0071	0.40	1.4
2×10^{-3}	0.12	0.21	0.38
10^{-3}	0.026	0.059	0.13
2×10^{-4}	0.074	0.38	0.15
10^{-4}	0.0069	0.0045	0.23
2×10^{-5}[b]	0.0073	0.0051	0.018
10^{-5}	0.0037	0.0012	0.28
2×10^{-6}[c]	0.049	0.072	0.095
10^{-6}	0.024	0.054	0.18
2×10^{-7}	0.25	0.52	0.99
10^{-7}	0.38	0.45	0.76

[a] Allowed relaxation time is 30 μs unless otherwise indicated. [b] 9 ms between pulses. [c] 30 ms between pulses.

etc. All values in Table II represent 30 μs allowed relaxation time between pulses, except at 2×10^{-5} Ω^{-1} and 2×10^{-6} Ω, where longer relaxation times were required to increase accuracy. The low capacitance values chosen represent a worst case since in most normal cells the series capacitance would be 1–3 orders of magnitude larger.

As a further test of the accuracy of the system for real conductance cells, data were acquired both with the computerized instrument and with a high-quality Wheatstone bridge (*11*). Several solutions were carefully prepared from very pure fused KCl and double-distilled, deionized water. The solutions which ranged in concentration from 0.1 to 0.005 M were placed in a traditional conductivity cell and allowed to reach temperature equilibrium at 25.00 ± 0.01 °C in a thermostat (Neslab Model TV 45/250). The resistances of the solutions were determined with both instruments. The average difference in the resistances was 0.02% and in no case was the difference greater than 0.04%.

Pulse Width Selection. In the selection of a particular pulse width for use in a given conductance region, two factors must be considered. First, the pulse width must be short compared to the time constant of the series RC formed by the double-layer capacitance and the solution resistance. Second, the pulse width must be long enough to allow the current follower to settle to its true output at the end of the pulsing. For low conductances the high current follower gain slows the response of the amplifier. Thus longer pulse widths must be used at lower conductances.

A plot of percent relative error vs. log R (for a series capacitance of 5 μF), covering the entire operating range, is shown in Figure 5. It is seen from the plot that, for best accuracy, the pulse width (PW) should be chosen as follows: below 10 kΩ, PW = 0.01 ms; between 10 and 70 kΩ, PW = 0.1 ms; between 70 and 700 kΩ, PW = 1.0 ms; and above 700 kΩ, PW = 10.0 ms. Similar curves were prepared for other series capacitances.

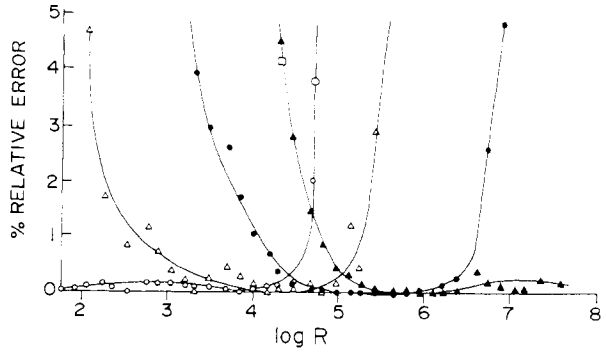

Figure 5. Percent error-vs.-log resistance at various pulse widths: (○) PW = 0.01 ms; (△) PW = 0.1 ms; (●) PW = 1 ms; (▲) PW = 10 ms

The curves are all in approximate agreement with the data of Figure 5 with regard to the proper choice of PW for a particular solution conductance. With these data as a basis, an algorithm was designed which selects the proper pulse width after the preliminary routine has been executed. The automated conductance system which we have described was applied to two illustrative chemical studies, the results of which are presented below.

APPLICATIONS WITH STOPPED-FLOW MIXING SYSTEMS

The following section describes the apparatus and two different chemical applications for the computerized conductance system. The temperature dependence of the first-order rate constant for the dehydration of carbonic acid has been determined and is compared with similar results obtained by other workers. The importance of temperature effects on measured conductances is emphasized by the results of a study of the reaction of nitromethane with base. Unless otherwise stated, all uncertainties in measured quantities are indicated at the 95% confidence level.

Apparatus. The rapid response and auto-ranging capabilities of the computerized conductance instrument make it nearly ideal as a detector in stopped-flow mixing experiments. To demonstrate this application of the instrument, the stopped-flow mixing system developed by Beckwith and Crouch (*12*) was used with the following modification. To provide conductometric detection and thermal detection, a multiple detector observation cell (*13*) was constructed and

installed in the instrument. The cell is somewhat different from conductometric cells described by others (*14–16*) in that it supports electrical conductance, optical absorbance, and thermal detection systems. The conductance electrodes are torus-shaped and were formed by sandwiching platinum disks between blocks of Kel-F and drilling a 2-mm horizontal flow channel through the entire assembly. The observation cell is sealed at each end by light pipes, and the Kel-F blocks are sealed by the pressure applied from each end by two threaded pieces which also contain the light pipes. The electrode configuration was arranged so as to provide several different possible cell constants but, in practice, the center two electrodes were found most useful.

The thermistor probe was constructed from a fast (τ = 7 ms) bead-in-glass thermistor (Thermometrics Corp.) and was connected to the fast temperature circuit via a shielded, 2-conductor cable. The optical detection system of the stopped-flow unit has been described elsewhere (*13*). The flow system has a dead time of ca. 3–4 ms (*17*).

Dehydration of Carbon Dioxide. One of the most extensively studied reactions by the stopped-flow technique is the dehydration of carbon dioxide which is shown in Equation 6.

$$H_2CO_3 \xrightarrow{k} H_2O + CO_2 \qquad (6)$$

The reaction is usually initiated by rapidly mixing acid and bicarbonate as shown in Equation 7.

$$H^+(aq) + HCO_3^-(aq) \overset{K}{\rightleftharpoons} H_2CO_3(aq) \qquad (7)$$

The reaction of Equation 7 is essentially instantaneous (k = 10^8 s^{-1} (*18*)), but the dehydration reaction is conveniently monitored by flow methods (*19–27*). The rate law expression has been derived elsewhere (*24*), and for conductometric detection, it has the following form:

$$[1 + (K/[HCO_3^-]_{ex})] \ln \delta_t + [1 - (K/[HCO_3^-]_{ex})] \ln \{([HCO_3^-]_{ex}/\beta) + \delta_t\} = kt + C' \qquad (8)$$

where

$$\delta_t = (G_t - G_\infty)/G_\infty \qquad (9)$$

$$\beta = 1000\ G_\infty\ \kappa/(\lambda_{HCO_3^-} + \lambda_{H^+}) \qquad (10)$$

and $C' = C + \ln \beta$ (*26*). In addition, K is the equilibrium constant for the reaction of Equation 7, $[HCO_3^-]_{ex}$ is the amount of bicarbonate in excess of the stoichiometric amount which is required to react with the acid, and C is a constant of integration. The other symbols have their usual significance: G is conductance; κ is the cell constant; and λ is the equivalent ionic conductance of the ion of interest.

A stock solution of ca. 0.1 M hydrochloric acid was prepared and standardized by the usual methods, and a solution of ca. 0.2 M sodium bicarbonate was prepared from the pure solid (*28*). The bicarbonate and acid solutions were mixed rapidly in the stopped-flow module, and at or near the time of the stop, data acquisition was initiated by a signal from an opto-interruptor module affixed to the stopping mechanisms (*13*). The averaged data were acquired and processed, and the resulting plots of G-vs.-time were displayed on the graphics display device. A sample data set is illustrated in Figure 6.

The interval over which the data were to be analyzed and the interval which was averaged to determine G_∞ values were chosen interactively from the terminal, and the analysis of the data was initiated. A linear least squares analysis of the left hand side of Equation 8 as a function of time was then performed, and the slopes, intercepts, standard deviations, standard errors of estimate, and correlation coefficients for the numerical analyses were presented on the display device.

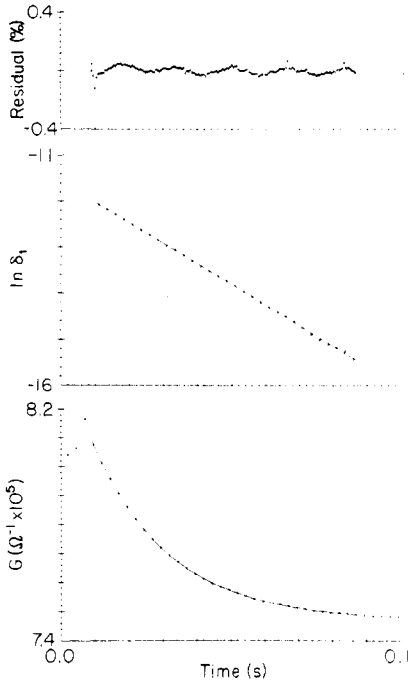

Figure 6. Reaction curve for the dehydration of carbonic acid by conductometric detection. Lower: (•) every tenth experimental point; (-) fitted exponential curve. Middle: (•) logarithmic plot, every tenth point; (-) least squares line. Upper: residuals ($G - G_{calcd}$)

Three experimental runs were made at each of five different temperatures. Since, as we have shown elsewhere (*29*), the temperature in the stopped-flow module does not change appreciably over the ~300 ms after the stop, no temperature compensation was necessary.

The quality of rapid reaction rate data obtained by the bipolar pulse conductance technique is clearly demonstrated in Figure 6. The quantities G, ln δ_t, and $G - G_{calcd}$ are presented as functions of time as are the linear least squares line for the logarithmic plot and the fitted exponential curve. The logarithmic plot is seen to be linear over at least five half-lives with a slope of −44.55 ± 0.13. The goodness of fit may be evaluated by determining the standard error of estimate, which for the data of Figure 6 was found to be 1.15 × 10^{-8} Ω^{-1}. This amounts to 0.21% of the total conductance change during the course of the reaction or 0.015% of the average conductance. This value is very close to the precision of a discrete conductance measurement. There is a small systematic variation in the residuals which may result from a line frequency component in the measured signal.

The first-order rate constants determined at the five different temperatures are illustrated in Figure 7 in the form of an Arrhenius-type plot of ln k-vs.-T^{-1}. These data may be compared to the results of Berger (*20*) obtained by the thermal and photometric stopped-flow techniques, the data of Roughton (*19*) resulting from continuous flow experiments with thermal detection, and the results of Dalziel (*22*) determined by continuous flow with photometric detection, all of which are also plotted in Figure 7. The precision of each rate constant is indicated by the vertical height of the plot symbol. The precision of the rate constants determined by conductometry ranged from 0.9% RSD to 2.5% RSD with an average of 1.7% RSD.

The values of ln k from this work are seen to lie on or very close to the best fit line through all of the data points. The activation energy, E_a, resulting from a weighted linear least squares regression analysis of the composite curve is 15.3 ± 0.3 kcal mol^{-1}, and E_a determined from the data which we have presented is 15.1 ± 0.6 kcal mol^{-1}. An analysis of the slopes

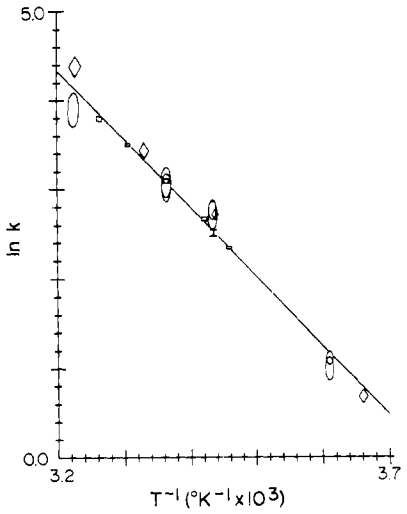

Figure 7. Arrhenius plot of rate constants obtained at various temperatures by conductometry and other techniques: (◊) thermal detection (*19*); (O) thermal and photometric detection (*20*); (I) photometric detection (*22*); (□) conductometric detection (this work). The heights of the plot symbols represent the uncertainties (± 1 *S*) in the ln *k* values

by the *t* test indicates that they are equal at the 99% confidence level. These experiments clearly demonstrate the suitability of the bipolar pulse conductance instrument for following the progress of rapid reactions.

The Reaction of Nitromethane with Base. As we have suggested elsewhere (*29*), temperature effects can be particularly important in stopped-flow mixing systems when the time course of the reaction is comparable to the time constant of the return of the observation cell to thermal equilibrium following the temperature change which often occurs during the push. This is especially true of conductometric detection since the conductance of an electrolyte solution may change by 1–3% per degree change in the temperature. A number of electronic schemes have been suggested (*1*, *30*) for correcting conductivity measurements for temperature changes.

The computerized conductance instrument with the capability of simultaneously acquiring precise temperature data provides a unique opportunity for numerical correction of conductivity data.

The procedure for numerically correcting measured conductance requires knowledge of the temperature-conductance behavior of the chemical system of interest. This is easily obtained by systematically varying the temperature of the reaction vessel (observation cell in the stopped-flow module) while simultaneously measuring the conductance and temperature of the reactant mixture as a function of time. The timed data acquisition program discussed in the Instrument section forms the basis for this type of study.

Once the *G*-vs.-*T* data have been acquired they are written into a data file on the disk. A least squares polynomial curve fit program is then called which stores the resulting coefficients in a file which may subsequently be read by other analysis programs. The temperature–conductance curves are seldom very complex over a reasonably narrow temperature range, and they can often be fit with a first-order equation. The fits are generally good to 0.05% of the measured conductance and are often good to better than 0.01% over narrow temperature ranges. Once the coefficients are obtained, all subsequent reactions in the same ionic medium may then be corrected by the analysis programs.

The temperature compensation process may be illustrated by the study of the reaction of nitromethane with base as shown in Equation 11.

$$CH_3NO_3 + OH^- \rightarrow CH_2NO_2^- + H_2O \qquad (11)$$

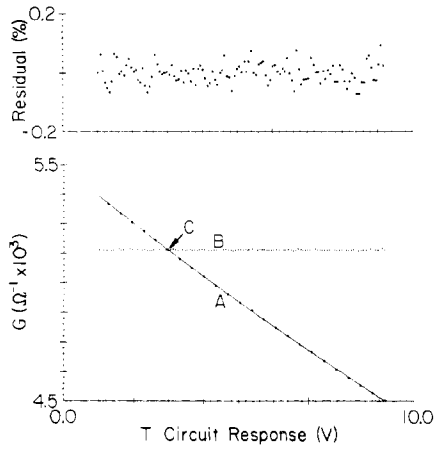

Figure 8. Conductance-vs.-temperature circuit response for a mixture of 5×10^{-5} M nitromethane and 3.36×10^{-3} M OH^-. Lower: Curve A: (*) every fifth experimental point; (-) fitted curve for third-degree polynomial. The equation for the curve may be found in the text. Curve B: conductance corrected to the temperature at point C. The numerical analysis of the curves is discussed in the text. Upper: residuals

The reaction may be conveniently carried out under pseudo-first-order conditions in excess base such that the reaction is complete in 40–60 s. This is about the same time scale as that of the thermal changes in our stopped-flow system (*29*).

A solution of ca. 10^{-2} M NaOH in double-distilled, deionized water was prepared and standardized against primary standard KHP. A solution 0.1 M in CH_3NO_2 was prepared from spectroquality nitromethane (Aldrich) and diluted to ca. 10^{-4} M. The solutions were combined, and the reaction was allowed to proceed to completion in the stopped-flow observation cell. The temperature of the equilibrium mixture was varied over a 10-K range, and the conductance and temperature were measured at 120 discrete points during the temperature change. The resulting data are shown in curve A of Figure 8.

A multiple regression analysis was carried out on the data, and an analysis of variance demonstrated that the most appropriate fitting function was a third degree polynomial. This analysis resulted in the following equation:

$$G(T) = 5.4895 \times 10^{-3} - 1.2431 \times 10^{-4}\, T + 2.4317 \times 10^{-6}\, T^2 - 7.1464 \times 10^{-8}\, T^3 \qquad (12)$$

The residuals for the fit, shown in Figure 8, were all found to be less than ±0.09% of the average value of the conductance, G_{av}. The standard error of estimate for the fitted curve was $1.45 \times 10^{-6}\ \Omega^{-1}$ or 0.03% of G_{av}.

Subsequent reactions with the same reactant solutions were carried out, and each measured conductance was corrected by using the coefficients from the curve fit, the measured temperature at each value of the conductance, and a standard temperature (usually the temperature over the first 100–300 ms of the reaction or the final equilibrium temperature) chosen interactively from the graphics terminal.

The success of the curve fitting technique can be illustrated by considering curve B in Figure 8. In this case the temperature to which the conductance measurements were corrected was the temperature of the mixture when the conductance had the value of the crossover point (point C) of the two curves. Thus a correction performed on the complete data set should give a horizontal line passing through the point. As curve B shows, the corrected conductance is constant to within ±0.08% (99.5% confidence) of the measured conductance at the crossover point, and the slope of the horizontal line is 1.4×10^{-8}. The intercept of the line is identical to the mean value of all of the points and is equal to 5.1391×10^{-3}.

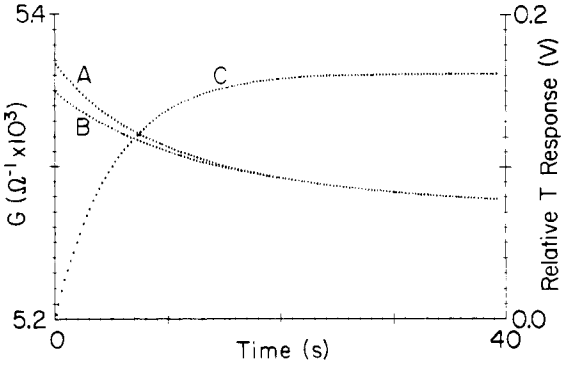

Figure 9. Conductometric curve showing the progress of the reaction of nitromethane with base. Curve A: raw data. Curve B: temperature corrected curve. Curve C: temperature response of stopped-flow mixing system. A discussion of the calculation of the rate constants may be found in the text

Figure 9 shows the result of a stopped-flow kinetics experiment on the same nitromethane system carried out at 25.0 °C. Curve A is the uncorrected conductance displayed as a function of time. Curve B is the conductance corrected for temperature changes which occurred during the progress of the reaction, and curve C is a typical response curve for the temperature monitor for our stopped-flow mixing system.

Pseudo-first-order rate constants calculated from a regression analysis of ln $(G - G_\infty)$-vs.-t for the two curves yield values of 10.7×10^{-2} s^{-1} for the raw data and 8.23×10^{-2} s^{-1} for the temperature corrected data. Since the concentration of base is known, the second-order rate constant under these conditions may be computed from the expression: $k_2 = k_1/[OH^-]$. This calculation yields values of 27.5 L mol^{-1} s^{-1} and 21.1 L mol^{-1} s^{-1} for the uncorrected and corrected rate constants, respectively; the difference being 23%. Both values are in reasonable accord with the value of 27.1 L mol^{-1} s^{-1} obtained by Knipe et al. (*31*) under somewhat different conditions, the value of 26.4 obtained by McLean and Tranter (*32*), the value of 27.6 found by Bell and Goodall (*33*) by a pH-stat method, and the value of 17.1 obtained both by an amperometric method (*34*) and by a high frequency method (*35*).

In addition, recent results by Campbell et al. (*36*) by constant rate titrimetry yielded values of 18.3, 21.7, and 35.6 at three different concentrations of nitromethane. The dependence of the rate constants on the concentration suggests that the reaction is probably not strictly pseudo-first-order, and it is therefore not possible to determine which of the curves of Figure 9 is more accurate. However, it is clear that a critical study of such reactions via the stopped-flow conductance technique will require careful examination of the data for possible temperature errors.

An important comparison may be made of the initial rates as determined from the uncorrected and corrected curves. This is especially pertinent if conductometric detection is to be used in reaction rate methods for the measurement of *initial* rates. That substantial errors can result when the effects of temperature are not taken into account, is demonstrated by the 51% difference in initial reaction rate between the two curves in Figure 9. It is, of course, the initial reaction rate that is more affected by the temperature change because of mixing (*29*).

ACKNOWLEDGMENT

The authors acknowledge the able assistance of T.V. Atkinson in the preparation of the figures. They are also indebted to Michael Kennedy of the University of Kentucky Department of Architecture for assistance in the treatment of some of the data.

LITERATURE CITED

(1) D. E. Johnson and C. G. Enke, *Anal. Chem.*, **42**, 329 (1970).
(2) D. E. Johnson, Ph.D. Thesis, Michigan State University, East Lansing, Mich., 1970.
(3) Frank M. Hussey, Master's Thesis, Michigan State University, East Lansing, Mich., 1971.
(4) P. H. Daum and D. F. Nelson, *Anal. Chem.*, **45**, 463 (1973).
(5) S. G. Ballard, *Rev. Sci. Instrum.*, **47**, 1157 (1976).
(6) F. J. Holler, S. R. Crouch, and C. G. Enke, *Chem. Instrum.*, **8**(2), 111 (1977).
(7) S. N. Deming and H. L. Pardue, *Anal. Chem.*, **42**, 1466 (1970).
(8) C. G. Enke and T. A. Nieman, *Anal. Chem.*, **48**, 705A (1976).
(9) A. Savitzky and M. J. E. Golay, *Anal. Chem.*, **36**, 1627 (1964).
(10) H. V. Malmstadt, C. G. Enke, S. R. Crouch, and G. Horlick, "Optimization of Electronic Measurements, Module 4", W. A. Benjamin, Menlo Park, Calif., 1974.
(11) H. Thompson and M. Rogers, *Rev. Sci. Instrum.*, **27**, 1079 (1956).
(12) P. M. Beckwith and S. R. Crouch, *Anal. Chem.*, **44**, 221 (1972).
(13) P. K. Notz, F. J. Holler, and S. R. Crouch, manuscript submitted.
(14) J. A. Sirs, *Trans. Faraday Soc.*, **54**, 201 (1958).
(15) R. H. Prince, *Trans. Faraday Soc.*, **54**, 838 (1973).
(16) M. A. Wolfe, *Chem. Instrum.*, **5**, 59 (1973).
(17) F. J. Holler, S. R. Crouch, and C. G. Enke, *Anal. Chem.*, **48**, 1429 (1976).
(18) M. Eigen, K. Kustin, and G. Mass, *Z. Phys. Chem.*, **30**, 130 (1961).
(19) Roughton, F. J. W., *J. Am. Chem. Soc.*, **63**, 2930 (1941).
(20) Berger, R. L. and Stoddart, L. C., *Rev. Sci. Instrum.*, **36**, 78 (1965).
(21) B. Balko, R. L. Berger, and Walter Friauf, *Anal. Chem.*, **41**, 4506 (1969).
(22) K. Dalziel, *Biochem. J.*, **55**, 79 (1953).
(23) R. L. Berger, B. Balko, W. Borcherdt, and W. Friauf, *Rev. Sci. Instrum.*, **39**, 486 (1968).
(24) R. Brinkmann, R. Margaria, and F. J. W. Roughton, *Philos. Trans. R. Soc. (London), Ser. A*, **232**, 65 (1933).
(25) J. A. Sirs, *Trans. Faraday Soc.*, **54**, 207 (1958).
(26) R. Saal, *Recl. Trav. Chim., Pays-Bas*, **47**, 264 (1928).
(27) C. Faurholt, *J. Chim. Phys.*, **21**, 400 (1924).
(28) T. Shedlovsky and D. A. McInnes, *J. Am. Chem. Soc.*, **57**, 1705 (1935).
(29) F. J. Holler, C. G. Enke, and S. R. Crouch, manuscript in preparation.
(30) T. R. Mueller, R. W. Stelzner, D. J. Fisher, and H. C. Jones, *Anal. Chem.*, **37**, 13 (1965).
(31) A. C. Knipe, D. McLean, and R. L. Tranter, *J. Phys. E: Sci. Instrum.*, **7**, 586 (1974).
(32) D. McLean and R. L. Tranter, *J. Phys. E*: Sci. *Instrum.*, **4**, 455 (1970).
(33) R. P. Bell and D. M. Goodall, *Proc. Roy Soc. London, Ser. A*, **294**, 273 (1966).
(34) E. W. Miller, A. P. Arnold, and M. J. Astle, *J. Am. Chem. Soc.*, **70**, 3971 (1949).
(35) P. J. Elving and J. Lakritz, *J. Am. Chem. Soc.*, **77**, 3217 (1955).
(36) B. H. Campbell, L. Meites, and P. W. Carr, *Anal. Chem.*, **46**, 386 (1974).

RECEIVED for review December 12, 1977. Accepted June 22, 1978. This work was supported in part by National Science Foundation Grants MPS 75-03650 and CHE76-81203.